Measurement of the ^{8}Li(α,n)^{11}B reaction and astrophysical implications

Y. Mizoi,* T. Fukuda, Y. Matsuyama, T. Miyachi,† and H. Miyatake
Institute for Nuclear Study (INS),‡ The University of Tokyo, 3-2-1 Midori-chou, Tanashi, Tokyo 188-0002, Japan

N. Aoi, N. Fukuda, M. Notani,* Y. X. Watanabe,* and K. Yoneda
Department of Physics, University of Tokyo, 7-3-1 Hongo, Bunkyou-ku, Tokyo 113-8654, Japan

M. Ishihara, H. Sakurai, Y. Watanabe, and A. Yoshida
The Institute of Physical and Chemical Research (RIKEN), 2-1 Hirosawa, Wako, Saitama 351-0198, Japan
(Received 27 December 1999; published 2 November 2000)

We have measured the ^{8}Li(α,n)^{11}B reaction directly and exclusively, and determined the total cross sections in the center-of-mass energy of 1.5–7.0 MeV, by using a new-type gas counter, multiple-sampling and tracking proportional chamber (MSTPC), and neutron counters. This experiment was performed in the condition of inverse kinematics. The ^{8}Li beam was produced by the RIKEN projectile-fragment separator, and injected into the MSTPC filled with ^{4}He gas, which worked as a detector gas and served as a target. The reaction cross section obtained in the present exclusive measurement is about half of the one obtained in previous inclusive measurements.

PACS number(s): 26.35.+c, 25.60.Dz, 25.70.Hi, 98.80.Ft

I. INTRODUCTION

The standard big-bang models (SM's) have succeeded in explaining the primordial nucleosynthesis of light elements. In these models, the predicted abundances of light elements up to $A=7$, which are presumed to be synthesized in the first three minutes of the hot big-bang expansion, are in good agreement with the observed ones in some interstellar regions, intergalactic clouds, and the atmospheres of the oldest-metal-poor stars, if the baryon density of the universe is $0.03 \leqslant \Omega_B h_{50}^2 \leqslant 0.06$. Here, Ω_B is the ratio of the present baryon density to the critical density, $\Omega_B = \rho_B / \rho_C$, h_{50} is the Hubble constant H_0 divided by 50 km/Mpc/sec, whose range is $0.8 < h_{50} < 2.0$, and ρ_C is the critical density which marginally closes the universe.

On the other hand, the total mass density of the universe, which is estimated by observations of the mass-luminosity ratio in the clusters or super clusters of galaxies on scales of $1 \sim 20$ Mpc, turns out to be $\Omega_0 = 0.3 \sim 1.2$ [1]. Here, the subscript 0 means the present value. The relation, $\Omega_B \ll \Omega_0$, suggests the existence of invisible mass, which is the so-called dark matter.

Recent observations [2] of rich clusters of galaxies have indicated a much larger baryon fraction, $\Omega_B / \Omega_0 = (0.2 \sim 0.3) h_{50}^{-3/2}$. In the marginally closed-universe model, $\Omega_0 = 1$, the baryon-density parameter becomes $\Omega_B = (0.2 \sim 0.3) h_{50}^{-3/2}$, which is many times larger than the SM's prediction. In another cosmological model of the flat universe $\Omega_0 + \Lambda_0 = 1$ with, for example, $\Omega_0 = 0.3$ and $\Lambda_0 = 0.7$, where Λ_0 is the cosmological constant, it becomes $\Omega_B = (0.06 \sim 0.09) h_{50}^{-3/2}$, being marginally consistent with the SM's prediction. However, it is controversial whether we need a finite Λ_0 or not, in order to make a model of the real universe, although a finite Λ_0 has become fashionable to account for acceleration of the universe expansion according to recent observations of the high-redshift supernovas [3,4],

Therefore, it is still important and critical to look for reasons that the observed baryon fraction, $\Omega_B / \Omega_0 = (0.2 \sim 0.3) h_{50}^{-3/2}$, may be larger than the SM's prediction, $0.03 \leqslant \Omega_B h_{50}^2 \leqslant 0.06$. On the other hand, inhomogeneous big-bang models (IM's), which allow larger $\Omega_B \sim 0.2 h_{50}^{-3/2}$ than the SM's, have been proposed and intensively studied [5–10].

One possible source of inhomogeneity is the quark-hadron phase transition occurring around 10^{-5} s after the big bang; a locally inhomogeneous baryon plasma may be produced by the quark-hadron phase transition, if the phase transition is first order. In addition, because the neutrons will diffuse out of the higher density regions of the baryon plasma more easily than the protons, which are attracted by the electrons, high-density regions that are proton rich and low-density regions that are neutron rich will be produced. In order to reproduce the observed light-element abundances, a higher baryon density of $\Omega_B \sim 0.2 - 1.0$ is required in the IM's, but ^{7}Li might be overproduced. However, recent astronomical observations of deuterium absorption line in Lyman-α clouds along the line of sight to high-redshift quasars have suggested a new interpretation of the observed ^{7}Li abundance [11]. Namely, the observed ^{7}Li abundance level in the oldest metal-poor stars is the result of large depletion from a higher primordial value consistent with the IM's prediction, and that both deuterium and lithium abundances can be explained in the IM's with $\Omega_B \sim 0.2$ [12].

A big difference in abundance is found for elements

*Present address: The Institute of Physical and Chemical Research (RIKEN), 2-1 Hirosawa, Wako Saitama 351-0198, Japan.

†Present address: The Japan Research Institute, Limited, 2-5 Ushijima-chou, Nishi-ku Nagoya 451-0046, Japan.

‡Present address: High Energy Accelerator Research Organization (KEK), 1-1 Oho, Tsukuba Ibaraki 305-0801, Japan.

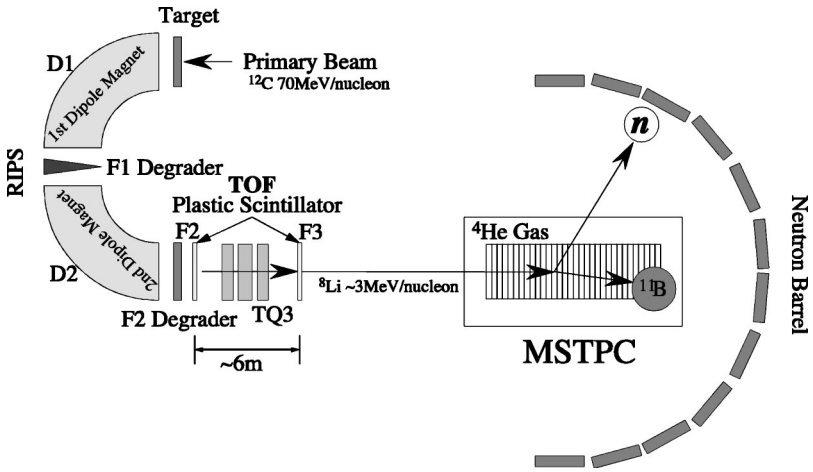

FIG. 1. Horizontal-plane schematic view of the experimental setup. The ^{8}Li beam was produced by the fragment separator, RIPS, and injected into the MSTPC with an energy of about 3 MeV/nucleon and an intensity of $1-2\times10^{3}$ s^{-1}. The MSTPC was filled with the ^{4}He gas, which served both as a detector gas and as a target. The neutron counters surrounding the MSTPC covered forward angles.

above $A=12$; namely, the abundances predicted by the IM's are much larger than those of the SM prediction by orders of magnitude, because neutron-rich nuclides play important roles in synthesizing heavier elements in an IM universe. The main path up to ^{12}C in IM nucleosynthesis is

$$^{1}\mathrm{H}(n,\gamma)^{2}\mathrm{H}(n,\gamma)^{3}\mathrm{H}(d,n)^{4}\mathrm{He}(t,\gamma)^{7}\mathrm{Li}(n,\gamma)^{8}\mathrm{Li}(\alpha,n)$$
$$^{11}\mathrm{B}(n,\gamma)^{12}\mathrm{B}(\beta\nu)^{12}\mathrm{C},$$

where ^{8}Li, whose half-life is 840 ms, is the key element. The three-body reaction $3\alpha\rightarrow{}^{12}$C is the main path to ^{12}C in SM nucleosynthesis.

In order to investigate IM's, the abundances of the elements must be calculated for entire reaction chains. However, the neutron-rich nuclides which occur in IM nucleosynthesis are mostly unstable against β decay; therefore, the experimental cross section data that are needed to calculate the nucleosynthesis are limited, because it is difficult to perform such cross-section measurements.

Two experiments designed to study the ^{8}Li$(\alpha,n)^{11}$B reaction have been performed, in spite of the difficulties caused by the short lifetime of ^{8}Li (840 ms). One experiment using the inverted reaction, ^{11}B$(n,\alpha)^{8}$Li, was performed by Paradellis *et al.* [13], which provided an excitation function of the ^{8}Li$(\alpha,n)^{11}$B(ground state) reaction. Other experiments involving an inclusive measurement of the ^{8}Li$(\alpha,n)^{11}$B reaction, with a multiple-sampling ionization chamber (MUSIC)-type detector [14], were performed by Boyd *et al.* [15] at RIKEN, and Gu *et al.* [16] at the Notre Dame–Michigan–Ohio State radioactive-beam facility. These experiments provide an excitation function of the ^{8}Li$(\alpha,n)^{11}$B reaction to all ^{11}B states. The observed cross section of the latter works is five times larger than that of the former at energy regions where their cross sections overlap. The discrepancy between them is attributed to the difference in the population of ^{11}B states involved; Ref. [13] measured only the ground-state reaction, while in Refs. [15,16], in principle, reactions into excited states of ^{11}B were also observed. However, the latter measurements did not observe the separate individual final states of the ^{8}Li$(\alpha,n)^{11}$B reaction.

In addition, Kubono *et al.* [17,18] and Mao *et al.* [19,20] measured the branching ratio from the excited states of the intermediate nucleus, ^{12}B, to the various states of ^{11}B through the ^{9}Be$(\alpha,p)^{12}$B*$(n)^{11}$B reaction. These experiments observed neutron decays from specific levels of ^{12}B* near an excitation energy of 10.6 MeV, which is within the Gamow peak for $T_9=1$, but the agreement between the two experiments is not good. In addition, their experiments may not populate all of the intermediate states relevant to the ^{8}Li$(\alpha,n)^{11}$B reaction.

Although there are some inconsistencies concerning the enhancement factor of the total cross section compared with the ground-state cross section derived from these experiments, it is reasonable to assume that the enhancement is caused by the population of excited states of ^{11}B. Therefore, in order to obtain the cross section of the ^{8}Li$(\alpha,n)^{11}$B reaction without ambiguity, exclusive measurements are needed. Hence, we performed, for the first time, such measurements with the multiple-sampling and tracking proportional chamber (MSTPC) [21], which has been designed to measure reactions involving unstable nuclides in the low-energy region.

II. EXPERIMENT

The experiment was carried out using the RIKEN projectile-fragment separator (RIPS) [22] at the RIKEN Accelerator Research Facility (RARF).

The experiment was designed for exclusive measurements of the ^{8}Li$(\alpha,n)^{11}$B reaction in order to determine the branching ratio to the various excited states as well as to the ground state of ^{11}B. Figure 1 shows a schematic view of the experimental setup, which consisted of an apparatus for producing low-energy radioactive isotope (RI) beams and detectors for measuring the reaction products. The former consisted of a fragment separator (RIPS) and an energy degrader, and the latter consisted of a time-of-flight (TOF) system for measuring the beam energy, neutron counters and the MSTPC filled with He gas which serves both as the target and the detector gas.

In order to verify the present experimental procedures, the ^{9}Be$(\alpha,n)^{12}$C reaction was also measured by the same system. The excitation function and branching ratios of the

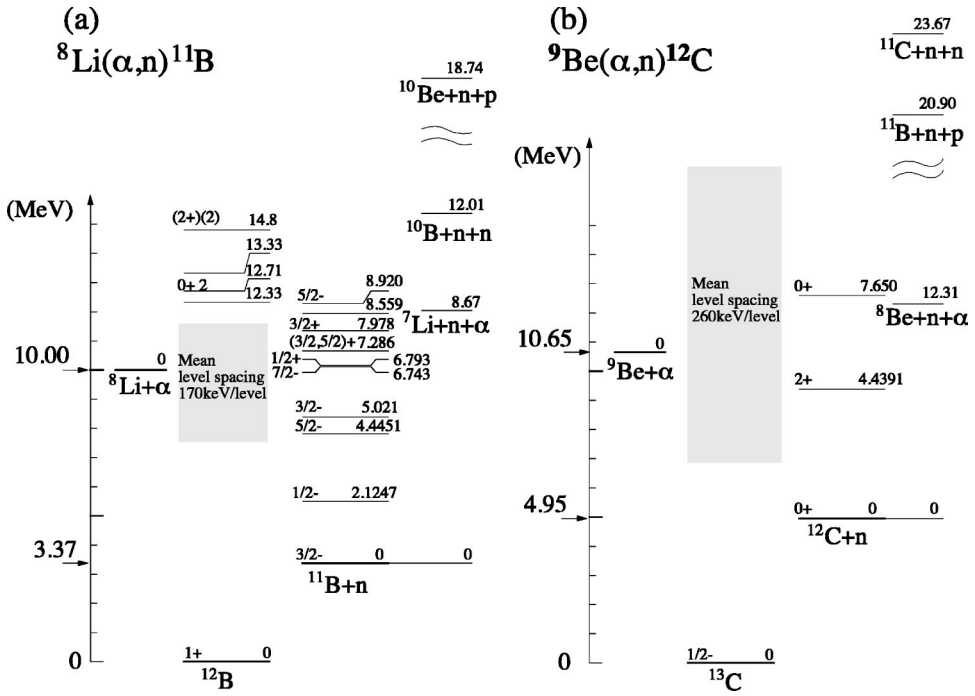

FIG. 2. Level schemes and properties of the nuclei involved in the ^{8}Li$(\alpha,n)^{11}$B and ^{9}Be$(\alpha,n)^{12}$C reactions. The vertical axis shows the reaction energy of the entrance channel and the excitation energies of the intermediate compound state or exit channels in unit of MeV. The respective ground states of the intermediate compound nuclei are set to be 0 MeV.

^{9}Be$(\alpha,n)^{12}$C reaction have been well measured [23–27]. The ^{9}Be$(\alpha,n)^{12}$C reaction is similar to the ^{8}Li$(\alpha,n)^{11}$B reaction in terms of the Q value ($Q_{^{8}\mathrm{Li}(\alpha,n_0)^{11}\mathrm{B(g.s.)}}=6.63$ MeV, $Q_{^{9}\mathrm{Be}(\alpha,n_0)^{12}\mathrm{C(g.s.)}}=5.7$ MeV) and the level structure, as shown in Fig. 2. The details of the individual apparatus are described in the following.

A. Low-energy RI beams

^{8}Li and ^{9}Be were produced through a projectile-fragmentation reaction with an incident ^{12}C beam on an 832 mg/cm^2 thick ^{9}Be target. The ^{12}C was accelerated to an energy of 70 MeV/nucleon, with an intensity of 60 pnA, by a four-sector ring cyclotron ($K=540$), following an AVF injection cyclotron ($K=70$). The RIPS has three focal planes: the first (F1) is the momentum-dispersive focal plane between the two dipole magnets (D1 and D2), where the achromatic degrader is located; the second (F2) and third (F3) are achromatic focal planes, with a triplet magnetic quadrupole lens (TQ3) system between F2 and F3. The other focusing elements, quadrupole magnets and sextupole magnets have been installed to correct higher-order beam optics.

The ^{8}Li and ^{9}Be isotopes were separated from other nuclides by the RIPS and collected in the second focal plane (F2) of the RIPS, where a 7 mm-thick Al plate for ^{8}Li and a 4 mm-thick Al plate for ^{9}Be were placed to degrade the energies of ^{8}Li and ^{9}Be down to 2–4 MeV/nucleon from $\sim$45 MeV/nucleon. The thickness of the Al plate traversed by the beam was adjusted by changing the angle of the plate with respect to the ion beam. The energy-degraded ^{8}Li and ^{9}Be were selected and collected on the third focal plane (F3) with rigidity specified by TQ3. The beam energies were measured by the TOF method between F2 and F3 with plastic scintillators. Finally, the ^{8}Li and ^{9}Be beams were injected into the MSTPC with an intensity of $1-2\times10^{3}$ s^{-1}. Figure 3 shows a TOF-energy plot of the ^{8}Li beams injected into the MSTPC. The horizontal axis is the TOF and the vertical axis is the energy measured by a Si solid-state detector (SSD), placed at the entrance of the MSTPC, for this calibration. The density plot and the solid curve indicate the measured data by the SSD and the calculated value corrected for any energy loss through the 64 μm-thick F3-plastic scintillator, respectively. The energies determined by the TOF system were consistent with the en-

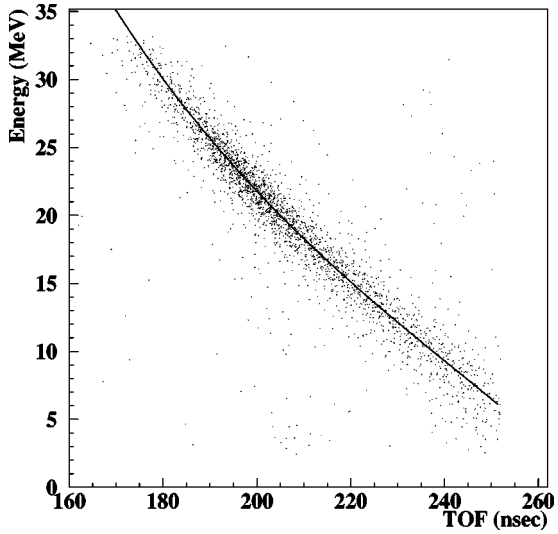

FIG. 3. TOF-energy plot of the ^{8}Li beam injected into the MSTPC. The solid curve shows the energies derived from TOF measured by the plastic scintillators placed at F2 and F3 of RIPS (see Fig. 1). The scatter plot shows the energies that were measured by the Si solid-state detector placed in the MSTPC and were corrected for the energy losses suffered in passing through the F3 plastic scintillator and the window film of the MSTPC entrance.

ergies measured by the SSD, and the energy resolution was about 1.2 MeV [full width at half maximum (FWHM)], which was mainly determined by the uniformity of the F3 plastic scintillator.

B. Detectors

The MSTPC and neutron counters were used for detecting reactions and measuring particle energies and spatial distributions. The MSTPC determined the reaction point and energy of the incident particles when the reaction occurred, and the neutron counters determined the neutron energy and angular distribution.

The MSTPC was developed for experiments with low-energy unstable-nucleus beams, and was designed based on the MUSIC-type detectors [14,28], which can measure the energy loss along the particle trajectories. The main advantage of the MUSIC-type detector is that the gas in the chamber works as both a detection medium and a gas target, a so-called active target, resulting in a high detection efficiency and a sufficient target thickness. Owing to these features of the MUSIC-type detector, reactions induced by unstable-nucleus beams with very limited intensities can be observed. In addition, the MSTPC has an advantage, which is the capability of the TPC (time-projection chamber) employing a flash ADC to identify multiple-track events. The details and performances of the MSTPC have been already reported in Ref. [21].

The ^{8}Li beams were injected into the MSTPC filled with gases of ^{4}He admixed with 5% (10%)-isobutane gas at about 400 torr pressure. Because the isobutane gas must be mixed with the ^{4}He gas for stable chamber operation, it can also act as a target. In order to estimate the background events by mixtures of ^{12}C and ^{1}H, 5% and 10% mixing ratios of isobutane gas were used. For a beam passing through the gases and the occurrence of a nuclear reaction, the energy loss (dE/dx) changes rapidly according to the change in its Z number; thus, the energy and position where the reaction occurs are determined by detecting the dE/dx change with the MSTPC.

The neutron counter consists of 12 vertical slats of plastic scintillator, BICRON BC408, each with an active area of 120 cm by 40 cm, and 2 cm thick. It has a barrel shape and a curvature center radius of 150 cm. The solid angle covered by each scintillator is 1.5% of 4π and the averaged intrinsic efficiency for a neutron at an energy region of 1.0–15 MeV is about 10%, estimated by Monte Carlo simulations coded by Cecil *et al.* [29]. This simulation code was optimized for the present neutron counter by Sasaki *et al.* [30], while considering the shape of the neutron counter and the measured light attenuation in plastic scintillator. The results of the simulation were fully examined by other experiments [31,32], measuring β-delayed neutrons from ^{17}N. In order to estimate the absolute efficiency, measurements with a ^{252}Cf fission source were also performed. The energy-threshold level was determined by measuring the neutrons from the fission source, and was set to be about 20 keV in electron-equivalent energy (20 keV e.e.), which corresponds to a neutron energy of about 0.5 MeV. Figure 4 shows the detection

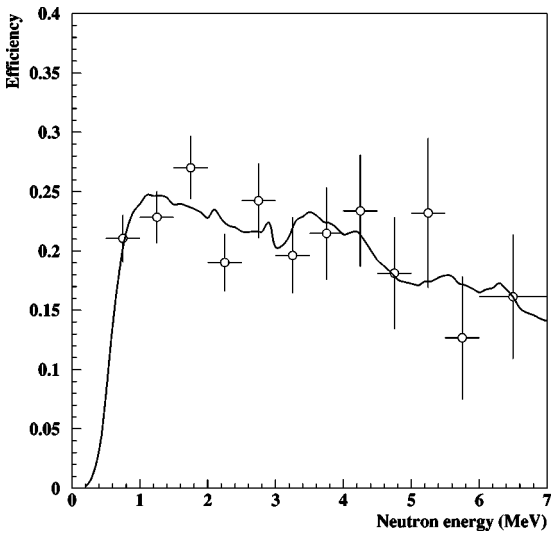

FIG. 4. Efficiency of the neutron counter as a function of the neutron energy. The open circles show the measured efficiencies with a ^{252}Cf fission source. The vertical error bars show the statistical error and the horizontal error bars show the energy-bin size. The solid curve shows the efficiency calculated by the computer simulation.

efficiencies which were obtained by the measurement of the ^{252}Cf-fission-source neutron, together with those by computer simulation. They are consistent with one another.

The neutron counters surrounded the MSTPC, symmetrically covering from 0 to ± 90 degrees, as shown in Fig. 1. The distance from the center of the MSTPC to the neutron counters was 1.5 m. The angular distribution of the neutrons was forward peaked because of the fast center-of-mass velocity of the colliding system. The neutron energies in the forward direction, i.e., for laboratory angles smaller than 90 degrees, almost always exceed the 0.5 MeV threshold energy of the neutron counter. In order to see this more clearly, the neutron energy distribution as a function of laboratory angle, when a reaction occurs at a center-of-mass energy of 2 MeV, is shown in Fig. 5. Almost all of the neutrons have energies larger than the threshold energy of the neutron counter (0.5 MeV), and will be detected. Only those n_8 neutrons that were emitted backward in the center-of-mass system would not be detected. Since only a small fraction of neutrons could not be detected, the systematic error due to the neutron energy threshold should be small.

III. ANALYSIS

The injected beam energies were determined by the TOF between F2 and F3, and were corrected for energy losses in the F3-plastic scintillator and the entrance window of the MSTPC. The beam energies on each cathode pad were derived by calculating the energy losses suffered in passing through the detector gases. The energy-loss calculations were performed by Ziegler's code [33] and small corrections were considered in order to represent the measured range in the mixed gases.

The reaction position and energy are determined by the position of the pad where the dE/dx change is detected in

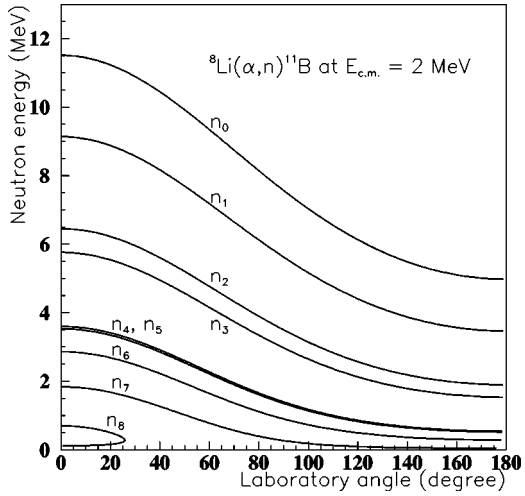

FIG. 5. Energy distribution of the neutrons. The energy of the neutron is plotted as a function of the laboratory angle, when a reaction occurs at the center-of-mass energy of 2.0 MeV. n_i means the group of neutrons emitted in the reaction leading to the ith excited state of ^{11}B.

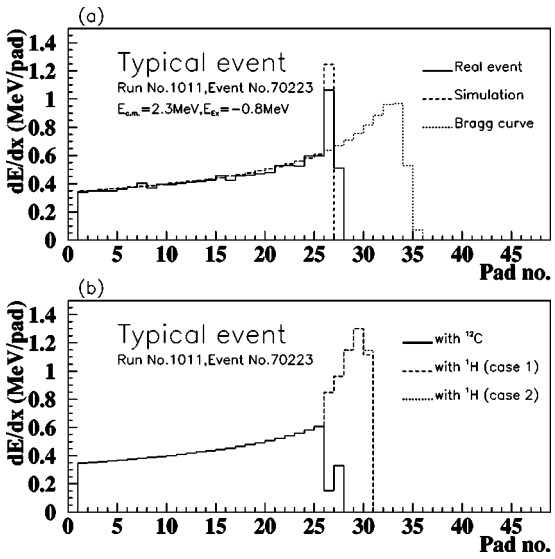

FIG. 6. Spectra of the dE/dx patterns for a typical event of the ^{8}Li(α,n)^{11}B reaction. (a) shows the dE/dx spectrum of a real event (solid curve) and that of a simulated one (dashed curve) generated from the measured information. Since they agree very well with one another, this event is regarded as a true ^{8}Li(α,n)^{11}B-reaction event. This event occurred at a center-of-mass energy of 2.3 MeV, which was determined by the MSTPC. The excitation energy of ^{11}B was calculated from the measured energy and momentum of the ^{8}Li beam and the neutron, resulting in -0.8 MeV, which was taken to be the ground state of ^{11}B, because this was within the estimated FWHM of the ground-state energy of ^{11}B (see Fig. 8). The dotted curve shows the Bragg curve of the ^{8}Li beam. (b) shows the simulated dE/dx spectra for the case of a reaction with ^{12}C or ^{1}H. The solid curve shows the case of ^{8}Li reactions with ^{12}C. The dashed curve (case 1) shows the case of a reaction with ^{1}H, and two α particles that are emitted at 0 and 180 degrees in their rest-mass system. The dotted curve (case 2) shows the case of a reaction with ^{1}H, and two α particles are emitted at 90 degrees in their rest-mass system. Since the lower spectra do not agree with the upper ones, the event in the upper figure is considered to result from the ^{8}Li(α,n)^{11}B reaction.

the MSTPC. Once the reaction energy and position, and the neutron TOF are determined, the energy and momentum of ^{11}B can be derived from a kinematic calculation employing the known beam and neutron information. Figure 6 shows a typical event of the dE/dx spectrum. The upper figure shows the dE/dx spectrum of a real reaction event that agrees with that of the simulated one. The simulated spectrum is generated from the beam, and the neutron energy and momentum information. Simulated reactions with a contamination like ^{12}C or ^{1}H are shown in the lower figure. They differ strongly with the dE/dx spectrum of the real reaction event. Therefore, the typical event is identified as a true ^{8}Li(α,n)^{11}B-reaction event.

Figure 7 shows the total cross sections corrected for the efficiencies estimated by the computer simulations that were performed, taking into account all conditions such as the detector setup, detection resolutions, and the reaction properties. The efficiencies including the detection efficiencies and the analysis efficiencies were determined as a function of the reaction energy and the final state of ^{11}B, and were applied to the analyzed data according to the reaction energy and the final state. The detection efficiencies consist of the neutron-detection efficiency (10–20 %, see Fig. 4), the solid angle covered by the neutron counters ($\sim$20% of 4π), the efficiency for detecting a charged particle by the MSTPC ($\sim$100% for $Z>2$), and the solid angle covered by the MSTPC ($\sim$100%). The analysis efficiencies are defined as the ratio of events accepted by the off-line-analysis gate to the true events. Then, the overall efficiency was about 1.0–1.5% for the energy region from 1.5 to 7.0 MeV for all states of ^{11}B. Because ^{8}Li beams with sufficiently low and well-defined energies were not obtained, events that occurred below a beam energy of 1.5 MeV could not be analyzed.

Because the total number of events is small and the peak resolution is not sufficiently good to distinguish individual final states, the individual excitation functions of the cross section to single excited ^{11}B states cannot be determined. The total cross sections do, however, include all of the states from the ground state to the ninth excited state. Because excited ^{11}B states of the tenth and above decay almost entirely by α emission [34], it is reasonable to consider the ninth excited state and below. By comparing the 10% and 5%-isobutane-mixed-gas data, it was determined that the effect of background events caused by the admixed ^{12}C or ^{1}H is not significant.

We measured the momentum and energy of both the beam and the neutron, the invariant mass of ^{11}B* could be calculated by assuming that the target was a helium nucleus. By subtracting the ground-state mass of ^{11}B from the calculated invariant mass of ^{11}B*, the excitation energy of ^{11}B* was derived. Figure 8 shows the excitation-energy spectrum of ^{11}B, that was analyzed by this procedure, and summed over the energy region between 1.5 and 7.0 MeV in the center-of-mass system. Since the tenth excited state and above, ^{11}B states almost always decay by α emission

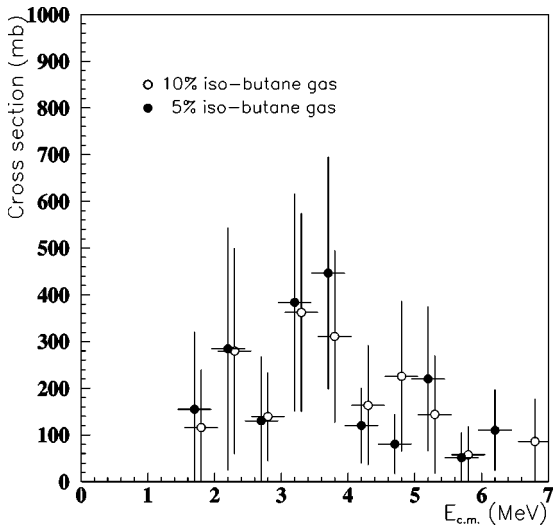

FIG. 7. Total-cross-section data for the ^{8}Li$(\alpha,n)^{11}$B reaction. The horizontal axis is the center-of-mass energy (MeV) and the vertical axis is the absolute cross section (mb). The open circles indicate the data for the 10%-isobutane-admixed gas, and the filled circles indicate the data for the 5%-isobutane-admixed gas. For clarity, the horizontal positions of the open circles are shifted by $+0.05$ MeV, and those of the filled circles by -0.05 MeV.

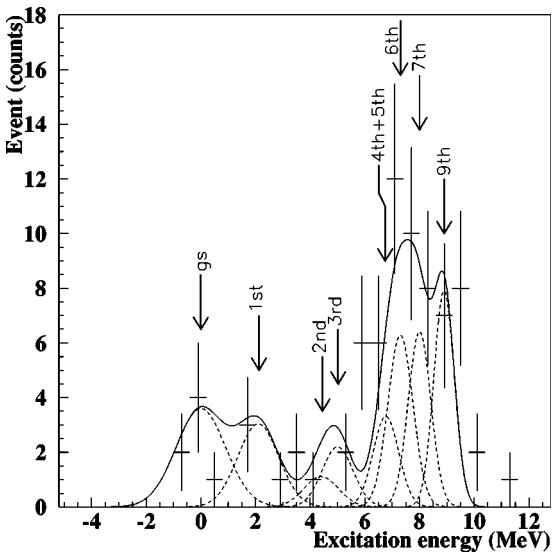

FIG. 8. Excitation-energy spectrum of ^{11}B. The horizontal axis shows the excitation energy in MeV and the vertical axis shows the number of raw events summed over the energy region between 1.5 and 7.0 MeV in the center-of-mass system. The solid curve is the result of a fit and the dashed curves show the individual components for the levels of ^{11}B. The crosses indicate the analyzed data; the horizontal error bars are the bin sizes and the vertical error bars are the statistical errors only. Because the tenth excited state and above, the ^{11}B states almost always decay by α-particle emission, i.e., $\Gamma_{\gamma}/\Gamma_{\alpha} \ll 1$, no event is seen above 12 MeV. The arrows indicate the levels of ^{11}B.

$(\Gamma_{\gamma}/\Gamma\alpha \ll 1$ [34]), such events could not form the required dE/dx patterns, and were rejected by the off-line analysis.

In order to determine the individual branching ratios, the response function derived from the simulations was used to fit the spectrum. The fitting result is plotted in Fig. 8. The branching ratios are derived by calculating the area of the individual peaks and taking the efficiencies determined by the computer simulations for each individual state. Table I gives the branching ratios which are the average ratios for the incident ^{8}Li energy range between 1.5 and 7.0 MeV in the center-of-mass system.

In order to evaluate the performance of the present experimental setup, the ^{9}Be$(\alpha,n)^{12}$C reaction, for which cross sections and angular distributions have already been well measured and are available, was also studied with the same experimental system as used in the ^{8}Li$(\alpha,n)^{11}$B reaction measurements. The measurements and analyses were performed by the same procedures and methods as those used for the ^{8}Li$(\alpha,n)^{11}$B reaction. The results are given in Table II. In the case of the ^{9}Be$(\alpha,n)^{12}$C reaction, the second excited state of ^{12}C decays to 3α with essentially 100% probability. Therefore, only neutrons to the ground state and first excited state of ^{12}C were considered. They agree with Refs. [23–27], well within the statistical errors.

IV. RESULTS AND DISCUSSIONS

A. Cross sections

Figure 9 shows the present result of the averaged cross section of the 10%-isobutane-gas cross-section data and the 5%-isobutane-gas cross-section data, together with other cross-section data for comparison. The other data indicate the cross section of the ^{8}Li$(\alpha,n_0)^{11}$B(g.s.) measured by the inverted reaction [13], that of the inclusive measurements by using the MUSIC at RIKEN [15] and at the Notre Dame–Michigan–Ohio State radioactive-beam facility [16]. The present data for the exclusive measurements show a lower cross section than those of the inclusive measurements over the entire energy region. In order to compare them more easily, the cross sections averaged between the energies of 1.5 and 5.0 MeV are given in Table III. The ground-state cross section of the present data agrees with that of the inverted reaction measurement within the statistical errors.

The reason why the present exclusive measurements disagree with the previous inclusive measurements may be due to systematic errors relevant to the previous inclusive measurements. They estimated the misidentification of events like elastic scattering; however, the procedure to discriminate ambiguous events was not described clearly. On the other hand, elastic events and other such events could not contaminate the present data owing to the neutron trigger and the requirement of a kinematical reconstruction. Moreover the present data agree with the ground-state cross section measured by the inverted reaction within statistical errors, and the cross sections measured here for the ^{9}Be$(\alpha,n)^{12}$C reaction are also consistent with the known cross sections. For these reasons, we believe that we have minimized systematic errors in our measurements by utilizing the better performance of the MSTPC and with the use of neutron counters; together these should have produced a highly restrictive event selection.

TABLE I. Averaged branching ratio for neutron decay of states in ^{12}B populated in the ^{8}Li$(\alpha,n)^{11}$B reaction. The ^{11}B state branching ratios and their errors are shown.

State (MeV)	g.s. (0.00)	1st (2.12)	2nd (4.44)	3rd (5.02)	4th (6.74)	5th (6.79)	6th (7.29)	7th (7.98)	8th (8.56)	9th (8.92)
Ratio (%)	24.32±12.55	15.17±10.44	4.17±7.17	6.13±5.74	4th+5th=13.01±8.03		12.45±10.38	10.56±7.10	0.0±2.12	14.22±6.69

Theoretical calculations of the ^{8}Li$(\alpha,n)^{11}$B reaction cross section were performed by Rauscher *et al.* [35] and Descouvemont [36]. Rauscher *et al.* calculated both the cross section of the ^{8}Li$(\alpha,n_0)^{11}$B(g.s.) reaction and the total cross section of the ^{8}Li$(\alpha,n)^{11}$B reaction. Their calculations were done before the inclusive measurements were performed, and gave a total cross section that was larger than the ground-state cross section by a factor of about 1.3. Descouvemont also calculated both the ground-state cross section and the total cross section. According to his work, if the total cross section of the inclusive measurements was reproduced, the ground-state cross section was overestimated by a factor of about 1.5. It seems that the theoretical results predict a smaller ratio between the ground-state cross section and the total cross section than claimed in the inclusive measurement, and thus favor the present result with a similar small enhancement factor.

B. Reaction rate

We will apply the present result to the reaction-rate calculations. The most important energy region for the ^{8}Li$(\alpha,n)^{11}$B reaction is around a center-of-mass energy of 0.6 MeV, where the Gamow peak for $T_9=1$ is located. However, cross-section data below 1.5 MeV in the center of mass were not obtained in the present measurements, so that extrapolations using the ground-state cross section, derived from the inverted reaction, must be performed as the only lower energy extrapolation available to us. Here, we assume three cases; the first is that the ground-state cross sections are multiplied by a factor of 2.6, which is determined by comparing the total cross section measured by the present experiment and the ground-state cross section measured by the inverted reaction, averaged between center-of-mass energies of 1.5 and 2.0 MeV. The second is that the ground-state cross section is multiplied by a factor of 3.1, which is determined by comparing the total cross section measured by the present experiment and the ground-state cross section measured by the inverted reaction between center-of-mass energies of 1.5 and 5.0 MeV. The third is that the ground-state cross section is multiplied by a factor of 4.1, which is the ratio of the total cross sections to the ground-state cross sections in the present result, averaged between 1.5 and 5.0 MeV. However, it seems that a factor of 2.6 should be a better choice than 3.1 or 4.1, since the reactions to the higher excited states of ^{11}B, which cannot be populated in the lower energy region below 2.0 MeV, may be included for the factors of 3.1 and 4.1. On the other hand, Boyd [15] and Gu [16] suggested a factor of 5 in their papers. Because the present methods to calculate the enhancement factor may be different from theirs, we re-evaluated the enhancement and obtained a factor of 6 by comparing their cross sections [15,16] with the ground-state cross section [13] between the center-of-mass energies of 1.5 and 5.0 MeV. This factor is larger than any of the present cases. For both extreme cases of the present data, i.e., factors of 2.6 and 4.1, astrophysical S factors are calculated and illustrated in Fig. 10. The resonance states given in Ref. [13] are also indicated.

Figure 11 shows the present result of the ^{8}Li$(\alpha,n)^{11}$B reaction rate, $\langle\sigma v\rangle$, as a function of temperature around $T_9=1$. The solid curve shows the choice of a factor of 2.6 and the dashed curve shows the choice of a factor of 4.1. The result given by Gu *et al.* [16] is also plotted as the dotted curve.

The reaction rate obtained for a factor of 2.6 can be expressed as

$$N_a\langle\sigma v\rangle = T_9^{-3/2}[2.66\times10^5\exp(-4.41/T_9)+3.00\times10^8\times\exp(-6.73/T_9)]+1.02\times10^{13}\times\exp(-19.46/T_9^{1/3})+8.82\times10^9\times\exp(-19.47/T_9)\,\mathrm{cm}^3/\mathrm{s\ \ mole}, \quad (1)$$

and that for a factor of 4.1 can be expressed as

$$N_a\langle\sigma v\rangle = T_9^{-3/2}[1.30\times10^6\exp(-4.41/T_9)+5.24\times10^8\times\exp(-6.73/T_9)]+1.07\times10^{13}\times\exp(-19.46/T_9^{1/3})+1.23\times10^{10}\times\exp(-19.47/T_9)\,\mathrm{cm}^3/\mathrm{s\ \ mole}, \quad (2)$$

TABLE II. Cross sections averaged over center-of-mass energies between 2.0 and 5.0 MeV, for the ^{9}Be$(\alpha,n)^{12}$C reaction. The present data agree very well with the reference data [23,24,24–26] within statistical errors.

	Cross section (mb)		
State (MeV)	g.s. (0.00)	1st (4.44)	total
Reference	66.5	193.4	259.9
Present	56.2±39.8	183.8±53.7	240.1±66.8

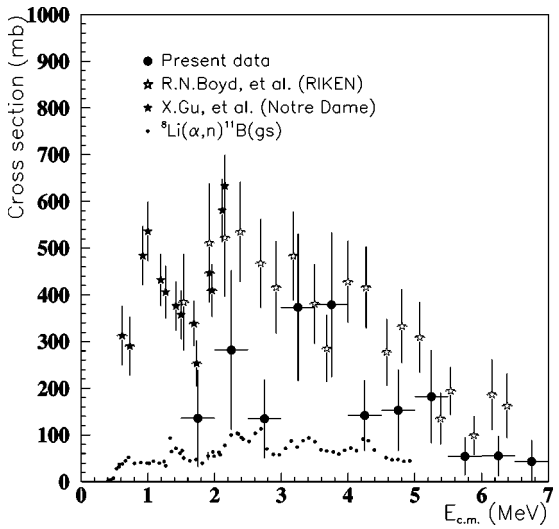

FIG. 9. Excitation functions for the ^{8}Li$(\alpha,n)^{11}$B reaction. The horizontal axis is the center-of-mass energy (MeV) and the vertical axis is the absolute cross section (mb). The filled circles indicate the present data averaged over the two mixing ratios of isobutane (Fig. 5). The small dots indicate the ground-state cross sections [13]. The open stars and filled stars indicate the data of the inclusive measurements [15,16].

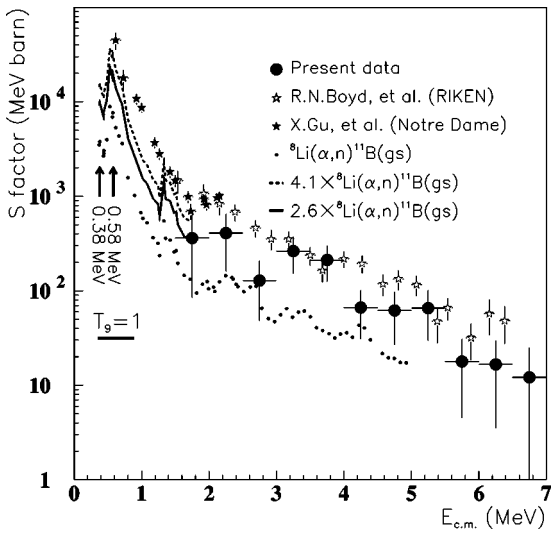

FIG. 10. Astrophysical S factor of the ^{8}Li$(\alpha,n)^{11}$B reaction. The horizontal axis is the center-of-mass energy (MeV) and the vertical axis is the astrophysical S factor (MeV barn). The filled circles are the present data, the open and filled stars are the inclusive-measurement data, and the small dots are the ground-state data. The extrapolated data using the ground-state cross sections [13] multiplied by factors of 2.6 and 4.1, below 1.5 MeV, are shown by the solid curve and the dotted curve, respectively.

where N_a is Avogadro's number. These reaction rates were derived by fitting the present result with the standard form described in Ref. [37]. The first and second terms are contributed by the resonance states at $E_r=0.38$ and 0.58 MeV, respectively. The third and fourth terms are contributions from the continuum for below and above the top of the Coulomb barrier, respectively. The two equations have different temperature dependences according to the assumed contributions of the cross sections extrapolated into the low-energy region.

V. SUMMARY AND OUTLOOK

The total cross sections and branching ratios of the ^{8}Li$(\alpha,n)^{11}$B reaction, which were not obtained simultaneously by previous experiments, were determined in the present work. The present measurements suggest that the ratio of the total cross section to the ground-state cross section is a factor of 2.6, which is lower than that of the inclusive measurements, estimated in earlier work as a factor of 5, or a factor of 6 as our reestimate of the ratio from the earlier work.

In a recent theoretical work performed by Terasawa *et al.* [38], it was quantitatively shown that the reaction chain, $\cdots{}^7$Li$(n,\gamma)^8$Li$(\alpha,n)^{11}$B$\cdots$, should also play an important role in addition to the previously identified process, $\cdots{}^4$He$(\alpha n,\gamma)^9$Be$(\alpha,n)^{12}$C$\cdots$, in the promising site for *r*-process nucleosynthesis caused by the neutrino-driven winds from the hot neutron star that is born right after the

TABLE III. Cross sections averaged over center-of-mass energies between 1.5 and 5.0 MeV for the ^{8}Li$(\alpha,n)^{11}$B reaction. The upper row is the present data and the lower row is data derived from the inverted-reaction measurement. The ground-state cross section of the present data was calculated using the branching ratio given in Table I.

	Cross section (mb)	
	Total	Ground state
Present	228.3±47.1	55.52±30.85
Inverse		74.07±0.33

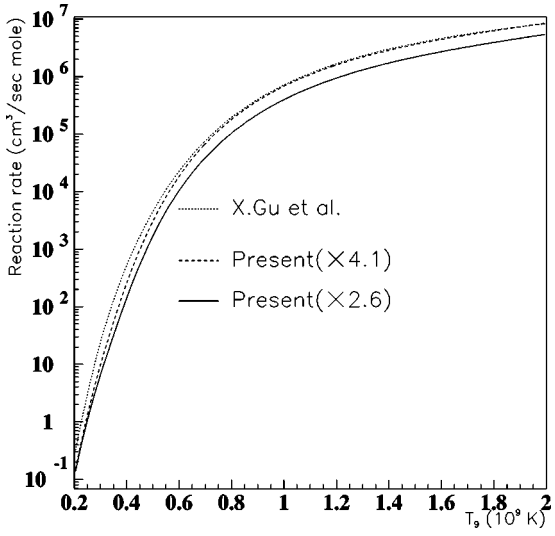

FIG. 11. Reaction rate of the ^{8}Li$(\alpha,n)^{11}$B reaction as a function of temperature. The horizontal axis shows the temperature T_9 (10^9 K), and the vertical axis shows the reaction rate in units of cm^3/s mole.

core collapse of a type-II supernova explosion. Therefore, the cross sections of the ^{8}Li(α,n)^{11}B reaction in the low-energy region also becomes important for testing this.

ACKNOWLEDGMENTS

The authors express their great appreciation to Dr. Y. Yamamoto, CNS University of Tokyo, and Professor T. Kajino, NAO Japan for much theoretical advice about the IM big bang. Sincere gratitude is extended to the staff members of RARF for their operation. Y.M. gratefully acknowledges the support of RIKEN. This work was supported in part by a Grant-in-Aid for Scientific Research on Priority Areas (Grant No. 05243102) of the Japanese Ministry of Education, Science, Sports, and Culture.

[1] N. A. Bahcall, L. M. Lubin, and V. Dorman, Astrophys. J. Lett. **447**, 81 (1995).
[2] L. P. David, C. Jones, and W. Forman, Astrophys. J. **445**, 578 (1995).
[3] A. G. Riess *et al.*, Astrophys. J. **116**, 1009 (1998).
[4] S. Perlmutter *et al.*, Astrophys. J. **517**, 565 (1999).
[5] C. Alcock, G. M. Fuller, and G. J. Mathews, Astrophys. J. **320**, 439 (1987).
[6] J. H. Applegate and C. J. Hogan, Phys. Rev. D **31**, 3037 (1985).
[7] J. H. Applegate, C. J. Hogan, and R. J. Scherrer, Phys. Rev. D **35**, 1151 (1987).
[8] T. Kajino and R. N. Boyd, Astrophys. J. **359**, 267 (1990).
[9] L. H. Kawano, W. A. Fowler, R. W. Kavanagh, and R. A. Malaney, Astrophys. J. **372**, 1 (1991).
[10] R. A. Malaney and W. A. Fowler, Astrophys. J. **333**, 14 (1988).
[11] D. Tytler, X. M. Fan, and S. Burles, Nature (London) **381**, 207 (1996).
[12] G. J. Mathews, T. Kajino, and M. Orito, Astrophys. J. **456**, 98 (1996).
[13] T. Paradellis, S. Kossionides, G. Doukellis, X. Aslanoglou, P. Assimakopoulos, A. Pakou, C. Rolfs, and K. Langanke, Z. Phys. A **337**, 211 (1990).
[14] K. Kimura, Y. Akiba, Y. Miake, and S. Nagamiya, Nucl. Instrum. Methods Phys. Res. A **297**, 190 (1990).
[15] R. N. Boyd, I. Tanihata, N. Inabe, T. Kubo, T. Nakagawa, T. Suzuki, M. Yonokura, X. X. Bai, K. Kimura, S. Kubono, S. Shimoura, H. S. Xu, and D. Hirata, Phys. Rev. Lett. **68**, 1283 (1992).
[16] X. Gu, R. N. Boyd, M. M. Farrell, J. D. Kalen, C. A. Mitchell, J. J. Kolata, M. Belbot, K. Lamkin, K. Ashktorab, F. D. Becchetti, J. Brown, D. Robers, K. Kimura, I. Tanihata, K. Yoshida, and M. S. Islam, Phys. Lett. B **343**, 31 (1995).
[17] S. Kubono, R. Boyd, N. Ikeda, M. H. Tanaka, T. Nomura, Y. Fuchi, H. Kawashima, M. Ohura, H. Orihara, S. Yun, H. Toyokawa, M. Yosoi, H. Ohnuma, I. Tanihata, and T. Kajino, Z. Phys. A **338**, 459 (1991).
[18] S. Kubono, N. Ikeda, M. H. Tanaka, T. Nomura, I. Katayama, Y. Fuchi, H. Kawashima, M. Ohura, H. Orihara, C. C. Yun, Y. Tajima, M. Yosoi, H. Ohnuma, H. Toyokawa, H. Miyatake, T. Shimoda, R. N. Boyd, T. Kubo, I. Tanihata, and T. Kajino, Z. Phys. A **341**, 121 (1991).
[19] Z. Q. Mao, R. B. Vogelaar, and A. E. Champagne, Nucl. Phys. **A567**, 111 (1994).
[20] Z. Q. Mao, R. B. Vogelaar, A. E. Champagne, J. C. Blackmon, R. K. Das, K. I. Hahn, and J. Yuan, Nucl. Phys. **A567**, 125 (1994).
[21] Y. Mizoi, T. Fukuda, Y. Matsuyama, T. Miyachi, J. Nakano, N. Fukuda, M. Hirai, H. Kobinata, Y. X. Watanabe, H. Sakurai, Y. Watanabe, and A. Yoshida, Nucl. Instrum. Methods Phys. Res. A **431**, 112 (1999).
[22] T. Kubo, M. Ishihara, N. Inabe, H. Kumagai, I. Tanihata, K. Yoshida, T. Nakamura, H. Okuno, S. Shimoura, and K. Asahi, Nucl. Instrum. Methods Phys. Res. B **70**, 309 (1992).
[23] C. N. Davids, Nucl. Phys. **A110**, 619 (1968).
[24] K. W. Geiger and L. Van Der Zwan, Nucl. Instrum. Methods **131**, 315 (1975).
[25] A. W. Obst, T. B. Grandy, and J. L. Weil, Phys. Rev. C **5**, 738 (1972).
[26] P. R. Wrean, C. R. Brune, and R. W. Kavanagh, Phys. Rev. C **49**, 1205 (1994).
[27] L. Van Der Zwan and K. W. Geiger, Nucl. Phys. **A152**, 481 (1970).
[28] W. B. Christie, J. L. Romero, F. P. Brady, C. E. Tull, C. M. Castaneda, E. F. Barasch, M. L. Crawford, I. Flores, D. E. Greiner, P. J. Lindstrom, H. Sann, and J. C. Young, Nucl. Instrum. Methods Phys. Res. A **255**, 466 (1987).
[29] R. A. Cecil, B. D. Anderson, and R. Madey, Nucl. Instrum. Methods **161**, 439 (1979).
[30] M. Sasaki and H. Miyatake (private communication).
[31] N. Aoi, K. Yoneda, H. Miyatake, H. Ogawa, Y. Yamamoto, E. Ideguchi, T. Kishida, T. Nakamura, M. Notani, H. Sakurai, T. Teranishi, H. Wu, S. S. Yamamoto, Y. Watanabe, A. Yoshida, and M. Ishihara, Nucl. Phys. **A616**, 181c (1997).
[32] H. Miyatake, Y. Yamamoto, T. Shimoda, S. Tanimoto, S. Mitsuoka, H. Ueno, H. Izumi, H. Ogawa, K. Asahi, N. Aoi, Y. Mizoi, M. Notani, K. Yoneda, M. Ishihara, E. Ideguchi, A. Ozawa, T. Kubo, and T. Kishida, RIKEN Accel. Prog. Rep. **30**, 59 (1997).
[33] J. F. Ziegler, *Handbook of Stopping Cross-Sections for Energetic Ions in All Elements* (Pergamon, New York, 1980), Vol. 5.
[34] G. Hardie, B. W. Filippone, A. J. Elwyn, M. Wiescher, and R. E. Segel, Phys. Rev. C **29**, 1199 (1984).
[35] T. Rauscher, K. Grün, H. Krauss, and H. Oberhummer, Phys. Rev. C **45**, 1996 (1992).
[36] P. Descouvemont, Nucl. Phys. **A596**, 285 (1996).
[37] R. V. Wagoner, Astrophys. J., Suppl. **18**, 247 (1969).
[38] M. Terasawa, K. Sumiyoshi, T. Kajino, I. Tanihata, and G. J. Mathews, Astrophys. J. (submitted).